RSC Advances

PAPER

View Article Online
View Journal | View Issue

Cite this: *RSC Adv.*, 2014, **4**, 47319

Gas sensing properties of flower-like ZnO prepared by a microwave-assisted technique

Xiaowei Li, Chen Wang, Xin Zhou, Jiangyang Liu, Peng Sun* and Geyu Lu*

Received 22nd July 2014
Accepted 8th September 2014

DOI: 10.1039/c4ra07425d

www.rsc.org/advances

Flower-like ZnO hierarchical architectures consisting of different building blocks have been successfully synthesized by a simple microwave-assisted decomposition route. The scanning electron microscopy and transmission electron microscopy results indicated that the morphologies of ZnO hierarchical architectures could be tailored by changing the category of the additives. Gas sensors based on the resulting products were fabricated and their gas sensing properties were tested for a variety of target gases. The results indicated that the sensor based on ZnO with a needle-assembled structure exhibited excellent selectivity and a higher response to NO_2 at 75 °C compared to those using the other two flower-like ZnO. The good performance observed here was likely to be the result of the high donor-related intrinsic defects.

1. Introduction

ZnO (zinc oxide), as a versatile semiconductor oxide, is extensively used in lithium batteries, luminescent materials, and solar cells.[1–3] With the increasing concern over safety in residential areas and environmental protection, gas sensors based on zinc oxide have attracted considerable attention because of their excellent gas-sensing properties. Recently, a variety of chemical and physical processes have been employed to fabricate zinc oxide microarchitectures, such as chemical vapor deposition (CVD),[4] thermal evaporation,[5,6] hydrothermal process[7,8] and Electrospinning.[9] However, time consuming procedures, sophisticated equipments, or rigid experimental conditions have limited the development of these methods. Microwave-assisted synthesis is a very attractive process for use in preparing functional material.[10] When radiation is applied to a solution containing reactants, one or more of them is capable of coupling with the microwave radiation. The charged particles then vibrate in the electric field of the radiation, thus faster heating is achieved, and the temperature and concentration gradients can be solved as well. Therefore, microwave-assisted synthesis has the advantages of homogeneous volumetric heating, high reaction rate, and energy savings as compared with conventional heating methods.

In addition, to get better understanding about the gas sensing mechanism, various theories and hypotheses have been proposed to try to figure out the nature of gas sensing in recent years. The most widely accepted theory for the gas sensing mechanism of metal oxides is based on the change in resistance, which proposed that the change in resistance of the sensor is caused by the chemical adsorption and the reaction of test gas molecules on the surface of the sensing materials.[11–13] However, gas sensing mechanism for semiconductor oxide is not yet fully understood, there are still many unknown factors affecting the sensing performance of gas sensor. Therefore, more works are needed to perfect the theory construction of gas sensing and the investigations of the comprehensive sensing mechanism still have importantly scientific and practical significance.

In this work, three kinds of flower-like zinc oxides were prepared by using a facile, green and efficient microwave-assisted decomposing method. The synthesis was conducted by exposing the mixed aqueous solutions including zinc acetate dihydrate, aqueous ammonia and different additives to microwave radiation with short reaction time (10 min) and low energy consumption (300 W). The gas sensing properties of the sensors based on these flower-like zinc oxides to 1 ppm NO_2 were investigated. Results show that the gas sensing performance varied with the morphologies of ZnO hierarchical structures, and the possible mechanism behind the discrepance of sensing performance was proposed based on the results of photoluminescence spectra.

2. Experimental

All chemicals used in this study were purchased from Beijing Chemical Reagent and directly used without further purification. In a typical synthesis process, zinc acetate dihydrate ($Zn(CH_3COO)_2 \cdot 2H_2O$, 0.44 g) and hexamethylenetetramine ($(CH_2)_6N_4$, 0.1 g) were added into 50 mL of deionized water with constant stirring for 30 min. Then 2 mL of aqueous ammonia

State Key Laboratory on Integrated Optoelectronics, College of Electronic Science and Engineering, Jilin University, Changchun, 130012, People's Republic of China. E-mail: spmaster2008@163.com; lugy@jlu.edu.cn; Fax: +86 431 85167808; Tel: +86 431 8516780

($NH_3 \cdot H_2O$, 30 wt%) was added into the above mixed solution. After further stirring for 5 min, the reaction mixture was transferred into a three-necked flask and placed in microwave synthesizer to irradiate for 10 min with the power set at 300 W (MAS-II, Shanghai Xinyi Ltd.). The precipitates were filtered, washed, and calcined at 500 °C for 2 h to obtain pure zinc oxide sample (named **S1**). The other two samples (**S2** and **S3**) were prepared with the same synthesis process, except that the additive of 0.1 g hexamethylenetetramine (HMT) was replaced by 0.1 g of hexadecyl trimethyl ammonium bromide (CTAB) and 1 mL of polyethylene glycol (PEG400), respectively.

The crystal structures and morphologies of samples were characterized by X-ray diffraction (XRD), field emission scanning electron microscopy (FESEM, JEOLJSM-7500F), selected-area electron diffraction (SAED), and high resolution transmission electron microscopy (HRTEM, JEM 2100F). Photoluminescence (PL) was measured from 370 to 600 nm at room temperature by a 320 nm excitation (Shimadzu RF-5301PC, Japan).

The detailed fabrication of chemical sensors were as follows: the as-prepared ZnO samples were mixed with deionized water to form a paste, and then coated on ceramic tube with a pair of gold electrodes and four platinum wires on both ends of the tube. A Ni–Cr alloy coil passed through the ceramic tube to control the working temperature by tuning the heating current. The structure of the sensor was schematically shown in Fig. 1a. Gas sensing measurements were processed by a static process in a test chamber under laboratory conditions (50 RH%, 22 °C), a conventional circuit was used to measure the change of resistance of the gas sensor (Fig. 1b). The response of the sensor was defined as the ratio between R_g (the resistance when exposed to test gas) and R_a (the resistance when exposed to air) for oxidizing gases or the reciprocal for reducing gases.

3. Results and discussion

3.1 Structural and morphological characteristics

The XRD patterns of the as-prepared zinc oxides are shown in Fig. 2a. Compared with the JCPDS Card no. 36-1451, all of the products could be indexed as the wurtzite hexagonal zinc oxide with lattice parameters of $a = 3.24982$ Å, $c = 5.2066$ Å (the space group: $P6_3mc$). No characteristic peaks of impurities or precursors were detected. The presence of sharp peaks in spectrum of **S1** indicates its higher degree of crystallinity after microwave irradiation as compared to those of **S2** and **S3**. The average

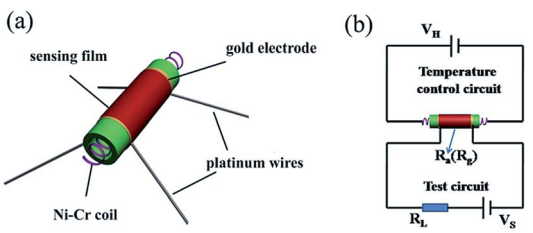

Fig. 1 (a) Schematic structure of the gas sensor; (b) schematic diagram of the electrical circuit for sensing test.

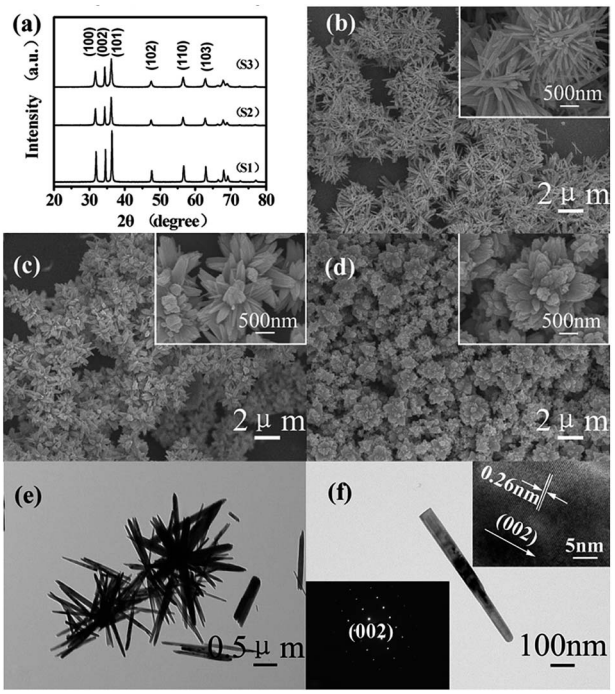

Fig. 2 (a) XRD patterns of the as-prepared ZnO; (b–d) SEM images of as-prepared ZnO (b) **S1**, (c) **S2** and (d) **S3**; (e and f) TEM images and SAED pattern of **S1**.

crystal size of **S1** was calculated to be about 30 nm using the Debye–Scherer formula ($D = 0.89\lambda/(\beta \cos \theta)$), where λ is the X-ray wavelength (1.5418 Å), θ is the Bragg diffraction angle, and β is the peak width at half maximum.

Fig. 2b shows the SEM image of **S1**, needle-assembled structure with flower-like morphology could be observed. The high-magnification SEM image indicates that the needle has an average length of about 1.5 μm and diameter of about 100 nm (inset of Fig. 2b). When 0.1 g of CTAB was used as additive, a bundle-like microstructures assembled by nanorods could be obtained, as shown in Fig. 2c. Changing the additive to PEG400 resulted in the flower-like hierarchical structures composed of some tight aggregations, as seen in Fig. 2d. It is obvious that the additive in experiment has great influence on the morphologies of as-synthesized ZnO products. The morphology and structure of **S1** was further characterized with TEM (Fig. 2e), which were in good accordance with the FESEM images. Fig. 2f presents the SAED pattern and HRTEM image of a single ZnO microneedle, it can be seen that the microneedle was single crystalline and grew preferentially along the c-axis corresponding to the [0001] direction. The adjacent lattice interplanar spacing was 0.26 nm, corresponding to the (0002) planes of the wurtzite ZnO.

Possible growth mechanism for flower-like ZnO was also investigated. During microwave irradiation, the hydroxyl ions are mainly provided by hydration of ammonia, which creates a strong base condition. The proposed reactions can be illustrated as follows:

$$NH_3 + H_2O \rightarrow NH_4^+ + OH^- \quad (1)$$

$$Zn^{2+} + 4OH^- \rightarrow Zn(OH)_4^{2-} \quad (2)$$

$$Zn(OH)_4^{2-} \rightarrow ZnO + H_2O + 2OH^- \quad (3)$$

It's well known that both pH and additives in solution are found to play important roles in determining the morphologies of products.[14] In our case, a large number of growth units $Zn(OH)_4^{2-}$ would be generated quickly, due to the high concentration of ammonia in solution (pH > 12). Thus, more growth units around the ZnO nuclei may lead to a faster growth kinetics which causes sheet defects such as twin boundaries of the ZnO crystals.[15] Because of the higher defect density and surface activity at these twin boundaries, the secondary nucleation will occur on the junction of these initial ZnO crystals,[16] leading to many polar (0001) surfaces will be exposed outside. With the preferential growth along the [0001] direction, flower-like ZnO can be obtained.[17] Moreover, the different appearance of flower-like ZnO can be attributed to the different additives. In the case of HMT, the basicity in the solution will increase due to hydrolyzing of HMT, the growth habit of ZnO is restricted to [0001] direction and leads to the formation of needle-assembled structure (Fig. 2f). When the CTAB is used, CTA^+ as a positively charged particle with a tetrahedral head and a long hydrophobic tail will form CTA^+–$Zn(OH)_4^{2-}$ ion pairs by electrostatic interaction with $Zn(OH)_4^{2-}$ ions. With the reaction keeping on, these ion pairs begin to self-assemble and change into bundle-like aggregated structure, which subsequently afford the formation of the ZnO assemblies after microwave irradiation.[14] If PEG400 is utilized, PEG400 molecules adsorb on ZnO nuclei surfaces and restrict the growth speed in all directions.[18] Consequently, some tight aggregations structures come into being under strong base condition. It is evident that the different additives have different functions in determining the growth speed and directions of ZnO crystals. The morphologies of products can be easily controlled by altering these additives in microwave-assisted synthesis.

3.2 NO_2 sensing properties

The responses of the sensors using as-obtained ZnO with different morphologies towards 1 ppm NO_2 were investigated and presented in Fig. 3. It can be seen that the optimum operating temperatures were 75, 150 and 100 °C for **S1**, **S2** and **S3**, respectively. Among the three sensors, the sensor using **S1** exhibited the largest response (R_g/R_a = 69) to 1 ppm NO_2 at 75 °C. Moreover, as can be seen in Fig. 4a–c, the sensor displayed more rapid response and recovery rate to 1 ppm NO_2 than other two sensors, likely because the loose architecture of **S1** provided abundant pores, which could enable the target gas to diffuse to the inner of sensing material quickly. The response and recover times of **S1** were 140 s and 320 s, respectively.

Fig. 5a shows the response transients of the sensors to 500 ppb nitrogen dioxide at 75 °C. It can be seen that all of the sensors maintained their initial response amplitude without a clear attenuation upon four periods tests, which indicated the good repeatability and stability of the sensors. The relationship between the responses of the sensors and NO_2 concentration

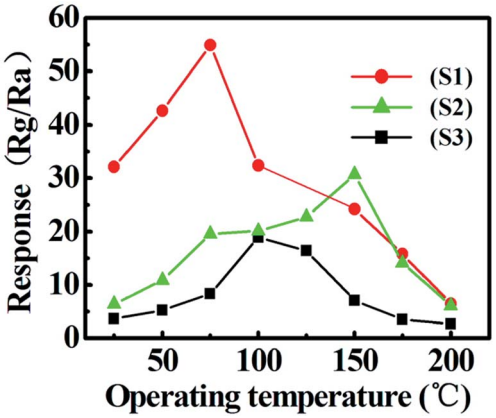

Fig. 3 Response of S1, S2 and S3 to 1 ppm NO_2 as a function of operating temperature.

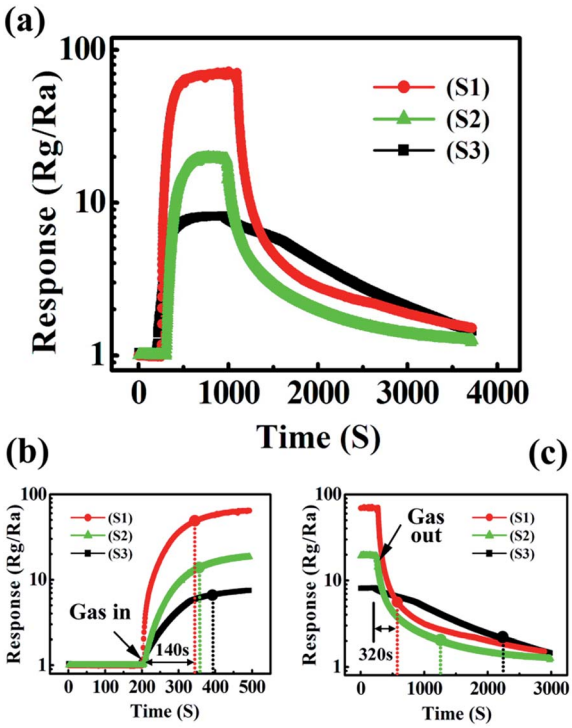

Fig. 4 Response and recovery characteristics of S1, S2 and S3 to 1 ppm NO_2 at 75 °C.

was presented in Fig. 5b, from which it can be seen that the sensor had a broad detection range to nitrogen dioxide from 100 to 1000 ppb and exhibited a low detection limit of 100 ppb to NO_2 gas.

Fig. 6 shows the responses of **S1** to various testing gases including chlorine, hydrogen sulfide, methane, acetone, ethanol and nitrogen dioxide. It is obvious that the sensor exhibited a markedly increase in the response of **S1** to NO_2 compared to other target gases, indicating its high degree of selectivity. It is well known that the interactions between test gases and metal oxide surface depend strongly on nature of materials and the category of tested gases. The optimal

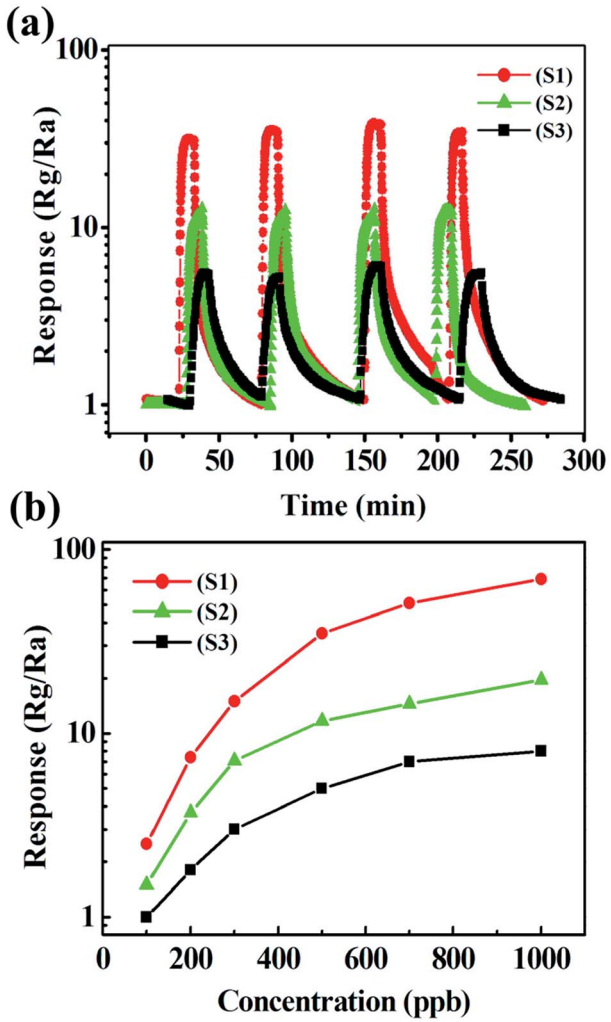

Fig. 5 (a) Reproducibility and transient response of the sensors to 500 ppb NO_2 gas; (b) response of the sensors *versus* the nitrogen dioxide concentrations at 75 °C.

operating temperature for different test gases is different. Thus, the high selectivity to NO_2 maybe arises from the fact that the selectivity was measure at optimal operating temperature to

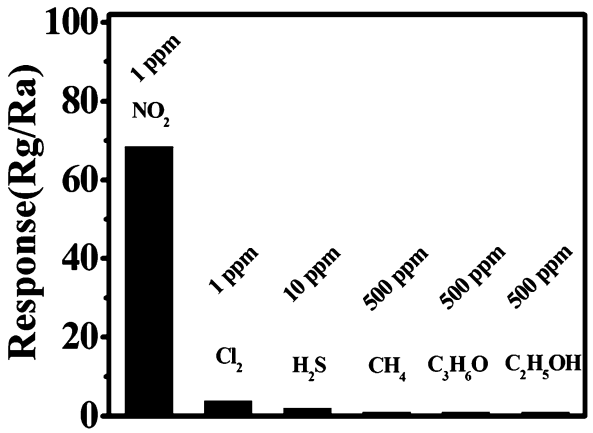

Fig. 6 Response of **S1** to various test gases.

nitrogen dioxide. A comparison between the sensing performances of the sensor and previously reported results is summarized in Table 1. It is noteworthy that the sensor fabricated in our work exhibits better sensing properties compared with those reported in the literature.[19–22]

3.3 PL spectra and mechanism for gas sensitivity

Some researchers have demonstrated that the intrinsic defects of ZnO may play an important role in determining its gas-sensing properties.[23,24] ZnO is believed to have five intrinsic defects: zinc interstitial (Zn_i), oxygen vacancy (V_O), zinc vacancy (V_{Zn}), oxygen interstitial (O_i) and oxygen antisite (O_{Zn}). Zn_i and V_O release free electrons (*i.e.* donor), while V_{Zn}, O_i and O_{Zn} consume free electrons (*i.e.* acceptor) in ZnO crystal.[25,26] It is known that PL spectrum of material originates from either the photoinduced electron–hole recombination or the intrinsic defects.[27] Therefore, we used the PL spectroscopic method to study the content of the defects. Fig. 7 presents the PL spectra of **S1**, **S2** and **S3** and their Gaussian decompositions. According to their originations, the donor-related (DL) peaks located near at 402 nm and 427 nm were attributed to Zn_i,[28] the peak located at 490 nm was oxygen vacancy (V_O).[28] Acceptor-related (AL) subpeaks located at 460 nm, 520 nm and 550 nm could be due to V_{Zn}, O_{Zn} and O_i, respectively.[24,29] We can learn that for the **S1**, **S2** and **S3**, the contents of donor defects and acceptor defects were (29.2%, 70.8%), (26.2%, 73.8%) and (24.1%, 75.9%), which has been summarized in Table 2. It is worth noting that the increasing sequence of donor-related subpeaks content (**S3** < **S2** < **S1**) was in accordance with the order of the gas sensing property (**S3** < **S2** < **S1**). Therefore, it is believed that the donor-related defects may play an important role in determining the gas sensing performance.

A popular and widely accepted sensing mechanism for n-type semiconductor oxides is based on the modulation of the depletion layer by oxygen absorption. When the sensor is exposed to air, oxygen molecules are adsorbed on the surface of the sensor and go on to be ionized by electrons from the materials conduction band to form oxygen species (O_2^-, O^- and O^{2-}). Electron depletion layers are formed on the sample surface. On exposure to an oxidative gas such as NO_2, these gas molecules will accept electrons through the surface reactions, increasing the width of surface charge layers. Thus, the sensor resistance is increased. Because of the important effect of intrinsic defects on gas-sensing properties, the probable sensing mechanism between ZnO and NO_2 can be mainly depicted as[30]

$$V_O + O_2(g) \leftrightarrow O_2^-(ads) + V_O^{\cdot} \quad (4)$$

$$2NO_2 + O_2^-(ads) + V_O^{\cdot} \leftrightarrow 2NO_3^-(ads) + V_O^{\cdot\cdot} \quad (5)$$

$$NO_2 + Zn_i \leftrightarrow NO_2^-(ads) + Zn_i^{\cdot} \quad (6)$$

$$NO_2 + NO_2^-(ads) + Zn_i^{\cdot}\cdots O_2 \leftrightarrow 2NO_3^-(ads) + Zn_i^{\cdot\cdot} \quad (7)$$

here "g" and "ads" refer respectively to gas and adsorption, $V_O^{\cdot}(Zn_i^{\cdot})$ represents single electropositive oxygen vacancy (zinc interstitial) and $V_O^{\cdot\cdot}(Zn_i^{\cdot\cdot})$ represents double electropositive

Table 1 Comparison of the sensing performances between the current work and previously reported results

Materials	Nitrogen dioxide	Operating temperature	Sensitivity	Limit of detection	Reference
ZnO nanonods	40 ppm	400 °C	206	—	19
ZnO nanofibers	4 ppm	200 °C	30	400 ppb	20
ZnO flower	5 ppm	200 °C	~78	500 ppb	21
ZnO nanonods	1 ppm	350 °C	1.8	~1 ppm	22
This work	1 ppm	75 °C	69	100 ppb	

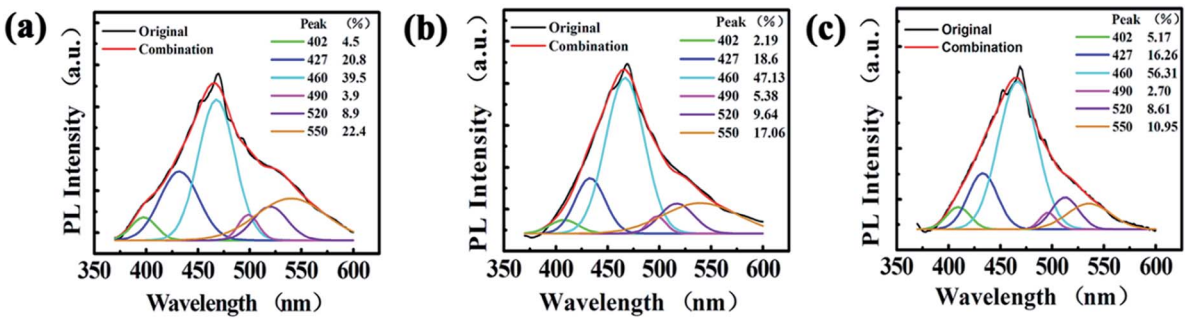

Fig. 7 Gaussian decomposed PL spectra of the flower-like ZnO (a) **S1**, (b) **S2**, (c) **S3**.

Table 2 The content of different intrinsic defects (%)

	Zn_i		V_O	Donor defects	V_{Zn}	O_{Zn}	O_i	Acceptor defects
S1	4.5	20.8	3.9	29.2	39.5	8.9	22.4	70.8
S2	2.19	18.6	5.38	26.2	47.13	9.64	17.06	73.8
S3	5.17	16.26	2.7	24.1	56.31	8.61	10.95	75.9

oxygen vacancy (zinc interstitial). According to the above equations, it can be seen that the donor-related intrinsic defects including Zn_i and V_O are helpful to enhance the gas response. Thus, **S1** possesses the highest response among the three samples, likely due to the highest content of donor-related defects and the lowest intrinsic acceptor-related defects.

4. Conclusions

Hierarchical ZnO nanostructures composed of different nanoscale building blocks have been prepared through microwave-assisted synthesis. By changing the category of additives, three kinds of flower-like shape ZnO with regular morphology and excellent crystallinity were obtained. A study on their gas-sensing properties reveals that the sensor based on **S1** exhibits outstanding selectivity, high response, rapid response and recovery behavior to NO_2, which is supposed to be arisen from the high contents of DL defects and low AL defects in its needle-assembled structure.

Acknowledgements

This work is supported by the National Nature Science Foundation of China (nos 61074172, 61134010, and 61327804) and Program for Chang Jiang Scholars and Innovative Research Team in University (no. IRT13018). National High-Tech Research and Development Program of China (863 Program, no. 2013AA030902 and 2014AA06A505).

Notes and references

1 H. Wang, Q. Pan, Y. Cheng, J. Zhao and G. Yin, *Electrochim. Acta*, 2009, **54**, 2851.
2 V. A. L. Roy, A. B. Djurišić, W. K. Chan, J. Gao, H. F. Lui and C. Surya, *Appl. Phys. Lett.*, 2003, **83**, 141.
3 A. B. F. Martinson, J. W. Elam, J. T. Hupp and M. J. Pellin, *Nano Lett.*, 2007, **7**, 2183.
4 J.-J. Wu and S.-C. Liu, *Adv. Mater.*, 2002, **14**, 215.
5 Z. R. Dai, Z. W. Pan and Z. L. Wang, *Adv. Funct. Mater.*, 2003, **13**, 9.
6 B. D. Yao, Y. F. Chan and N. Wang, *Appl. Phys. Lett.*, 2002, **81**, 757.
7 S. Baruah and J. Dutta, *Sci. Technol. Adv. Mater.*, 2009, **10**, 013001.
8 J. X. Wang, X. W. Sun, Y. Yang, H. Huang, Y. C. Lee, O. K. Tan and L. Vayssieres, *Nanotechnology*, 2006, **17**, 4995.
9 R. Siddheswaran, R. Sankar, M. Ramesh Babu, M. Rathnakumari, R. Jayavel, P. Murugakoothan and P. Sureshkumar, *Cryst. Res. Technol.*, 2006, **41**, 446.

10 M. Baghbanzadeh, L. Carbone, P. D. Cozzoli and C. O. Kappe, *Angew. Chem., Int. Ed.*, 2011, **50**, 11312.
11 N. Yamazoe, G. Sakai and K. Shimanoe, *Catal. Surv. Asia*, 2003, **7**, 63.
12 N. Yamazoe and K. Shimanoe, *Sens. Actuators, B*, 2009, **138**, 100.
13 M. Batzill and U. Diebold, *Phys. Chem. Chem. Phys.*, 2007, **9**, 2307.
14 J. Ge, B. Tang, L. Zhuo and Z. Shi, *Nanotechnology*, 2006, **17**, 1316.
15 X. W. Li, P. Sun, T. L. Yang, J. Zhao, Z. Y. Wang, W. N. Wang, Y. P. Liu, G. Y. Lu and Y. Du, *CrystEngComm*, 2013, **15**, 2949.
16 R. A. McBride, J. M. Kelly and D. E. McCormack, *J. Mater. Chem.*, 2003, **13**, 1196.
17 N. F. Hamedani, A. R. Mahjoub, A. A. Khodadadi and Y. Mortazavi, *Sens. Actuators, B*, 2011, **156**, 737.
18 X. Li, G. He, G. Xiao, H. Liu and M. Wang, *J. Colloid Interface Sci.*, 2009, **333**, 465.
19 S. Bai, X. Liu, D. Li, S. Chen, R. Luo and A. Chen, *Sens. Actuators, B*, 2011, **153**, 110.
20 J.-A. Park, J. Moon, S.-J. Lee, S. H. Kim, H. Y. Chu and T. Zyung, *Sens. Actuators, B*, 2010, **145**, 592.
21 J. Chang, M. Z. Ahmad, W. Wlodarski and E. R. Waclawik, *Sensors*, 2013, **13**, 8445.
22 P.-S. Cho, K.-W. Kim and J.-H. Lee, *J. Electroceram.*, 2006, **17**, 975.
23 L. X. Zhang, J. H. Zhao, H. Q. Lu, L. M. Gong, L. Li, J. F. Zheng, H. Li and Z. P. Zhu, *Sens. Actuators, B*, 2011, **160**, 364.
24 M. Chen, Z. Wang, D. Han, F. Gu and G. Guo, *J. Phys. Chem. C*, 2011, **115**, 12763.
25 J. L. Zhao, W. Zhang, X. M. Li, J. W. Feng and X. Shi, *J. Phys.: Condens. Matter*, 2006, **18**, 1495.
26 G. Y. Huang, C. Y. Wang and J. T. Wang, *J. Phys.: Condens. Matter*, 2009, **21**, 195403.
27 K. Samanta, P. Bhattacharya and R. S. Katiyar, *J. Appl. Phys.*, 2009, **105**, 113929.
28 S. Saha and V. Gupta, *J. Appl. Phys.*, 2011, **110**, 064904.
29 N. Han, P. Hu, A. Zuo, D. Zhang, Y. Tian and Y. Chen, *Sens. Actuators, B*, 2010, **145**, 114.
30 M. Chen, Z. Wang, D. Han, F. Gu and G. Guo, *Sens. Actuators, B*, 2011, **157**, 565.

